*Bulgarian Chemical Communications, Volume 54, Issue 4 (pp. 349-354) 2022 DOI: 10.34049/bcc.54.4.5539*

# Comparison of the model axial graphene strain distributions in graphene/epoxy/polymethyl methacrylate (PMMA) nanocomposite under mechanical and thermomechanical loading

R. K. Vladova*, T. S. Petrova, E. G. Kirilova, A.G. Apostolov, B. Ch. Boyadjiev

*Institute of Chemical Engineering, Bulgarian Academy of Sciences,*
*Acad. G. Bonchev Str., Bl.103, 1113 Sofia, Bulgaria*

Received: November 07, 2022; Revised: November 25, 2022

The current report presents a theoretical study of the application of a two-dimensional stress-function method to analytically describe and compare the strains in graphene/epoxy/polymethyl methacrylate (PMMA) nanocomposite structure under three types of loading - mechanical, thermal and thermo-mechanical. Respectively, three model case solutions for all 2D strains in the nanocomposite layers at different cases of loading are developed, considered and compared with each other to illustrate the temperature influence on the strains. All results for the behavior of the axial, peel and shear strains for all three layers of the structure are illustrated in figures and discussed.

The model axial strain in the graphene layer at two different mechanical external strains - 0.3% and 0.8%, was compared and validated with experimental data at mechanical loading. The obtained results could be used for fast prediction of strain distributions in similar nanocomposite devices as sensors, nano- and optical electronic devices, energy devices, etc., at different types of external loadings.

**Keywords:** 2D stress-function method, strain, comparison, analytical solutions, graphene-epoxy-PMMA nanocomposite

## INTRODUCTION

Research publications on the graphene-polymer nanocomposites, especially experimental ones, continuously increased exponentially both immediately - about 3000 [1] after the discovery of graphene and ten years later - about 10000 [2]. It is encouraging that in the recent years, the number of analytical and numerical approaches which have been employed to study the effect of graphene as reinforcement on the performance of polymer nanocomposites also continuously raised. Many methods and theories have been tried and approved such as molecular dynamics, continuum mechanics, atomistic simulation [3-5], multiscale modeling [6-8], etc.

In [9] the authors have reviewed the modelling of polymer nanocomposites reinforced with spherical nanoparticles or statistically isotropic aggregates. In [10] a 3D computational model of graphene-reinforced polymer composites has been developed and applied for the analysis of damage and fracture mechanisms in the composites. In [11] the interfacial stress transfer between a monolayer graphene and a commonly used PMMA matrix is studied under pristine vdW and modified H-bonding interactions by a proposed nonlinear shear-lag model. The latter considered friction beyond linear bonding, to understand evolution of interfacial stresses and further identify key interfacial parameters. In contrast to most finite element models [12-14] considering the matrix damage or the interfacial debonding in graphene-reinforced polymer nanocomposites and requiring high computational effort, the analytical models based on shear-lag analysis are much more efficient.

Such analytical models [15, 17, 18] are very suitable for the preliminary design of bonded structures and provide reasonable results very quickly, reduce test costs and analysis time. Up to now, most of published works [19, 24-29] attended with graphene-reinforced polymer nanocomposites, are mainly experimental.

Applying the shear-lag theory, it is reported [18], that if the polymer substrate is subjected to a relatively small strain, the classical shear-lag model is valid with a linear shear stress-sliding displacement relationship and the structure is perfectly bonded. Also, in [19] on the basis of the shear-lag analysis, it is shown that an efficient reinforcement can be realized only if the size of the graphene flake is large enough (more than 30 μm). When the structure is subjected to a larger strain, a nonlinear shear-lag model has to be applied [20-23].

Despite the large number of theoretical studies on graphene-PMMA nanocomposites, there are very few works related to the behavior of the same on thermal treating. So far, the following works were found where the influence of temperature was also investigated [5, 24-28, 30, 31].

* To whom all correspondence should be sent:
E-mail: r.vladova@iche.bas.bg

No work was found about how and why temperature affects stresses or strains in a structure. Our own contribution to the subject up to date is [32], in which the foundations were laid with a derived analytical solution for the stresses in the monolayer graphene/SU-8/PMMA layers in the presence of temperature and moisture, but the results were not validated due to lack of data. Therefore, in the present work, in addition to comparison and analysis of the different solutions with and without temperature effect for the deformations, a partial validation of the model results with data from [16] was done. The data used concerned the distribution of deformations in the graphene layer at external mechanical loads of 0.3% and 0.8%, without temperature influence. Unfortunately, available data are only for elastic loading; it is known that the critical value for the external strain applied for graphene monolayer without debonding is 0.53 % [17].

Here, the theoretical study of the application of a two-dimensional stress-function method is proposed, to analytically describe and compare the strains in a graphene/epoxy/polymethyl methacrylate nanocomposite structure under three types of loading - mechanical, thermal and thermo-mechanical. Respectively, three model case solutions for all 2D strains in the nanocomposite layers at different cases of loading were developed, considered and compared with each other to illustrate the temperature influence on the strains. The model axial strain in the graphene layer at two different mechanical external strains - 0.3% and 0.8%, was compared and validated with experimental data at mechanical loading.

*Model and developed analytical solutions for stresses and strains in the nanocomposite structure*

Usually, the graphene flake is embedded in the polymer matrix, in this way increasing the strength and toughness of the respective nanocomposite.

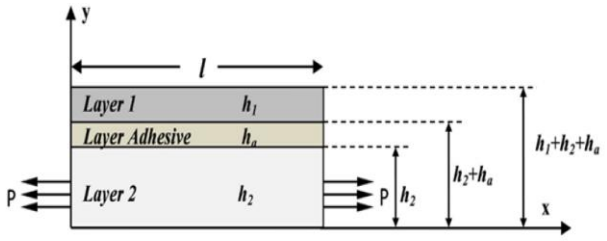


**Fig. 1.** Representative volume element (RVE) of graphene-(adhesive)-polymer nanocomposite structure

A representative volume element (RVE) is presented on Fig. 1. of the graphene-(adhesive)-polymer nanocomposite structure, where $l$ - the length of the overlap zone, $h_i$, (i) = 1, 2, a are the thicknesses of graphene, polymer and adhesive layers, P - the static tensile force.

The axial stresses in the layers are assumed to be functions of axial coordinate *x* only. In the adhesive interface layer, the axial stress is neglected, or $\sigma_{xx}^{(\alpha)} = 0$. All stresses in the layers (axial, normal (peel) and shear stresses) are determined under the assumption of the plane-stress formulation (standard constitutive strain-stress equations from 2D elasticity theory). The 2D stresses in the layers (axial, shear and normal) are obtained through integrating by *y* the differential equations of equilibrium and satisfying the boundary and contact conditions.

They are expressed in terms of a single stress potential function (axial stress of the graphene layer $\sigma_1$ and its first and second derivatives, as follows:

Layer 1:

$$\sigma_{\mathrm{x}}^{(1)} = \sigma_{1,} \quad \sigma_1' = \frac{d\sigma_1}{dx}, \quad \sigma_1'' = \frac{d^2\sigma_1}{dx^2},$$
$$\sigma_y^{(1)} = \frac{1}{2}\big(y - (h_1 + h_2 + h_a)\big)^2 \sigma_1'',$$
$$\sigma_{xy}^{(1)} = \big((h_1 + h_2 + h_a) - y\big)\sigma_1' \qquad (1)$$

Layer adhesive:

$$\sigma_{\mathrm{x}}^{(\alpha)} \equiv 0, \ \sigma_{xy}^{(\alpha)} = h_1\sigma_1'$$
$$\sigma_y^{(\alpha)} = \left[\frac{h_1^2}{2} + h_1(h_2 + h_\alpha - y)\right]\sigma_1'', \qquad (2)$$

Layer 2:

$$\sigma_{\mathrm{x}}^{(2)} = \sigma_0 - \rho\sigma_1, \qquad \rho = \frac{h_1}{h_2},$$
$$\sigma_y^{(2)} = \frac{-h_1}{2h_2}[y^2 - y(h_1 + h_2 + 2h_a)]\sigma_1'',$$
$$\sigma_{\mathrm{xy}}^{(2)} = \frac{h_1}{h_2} y\sigma_1 \qquad (3)$$

The complementary $W_i$ and total $W$ strain energy are obtained through integrating by *y* for each layer:

$$W_i = \frac{1}{2}\int_0^l \int_y \Big[\Big(\sigma_x^{(i)}.\varepsilon_x^{(i)} + \sigma_y^{(i)}.\varepsilon_y^{(i)} + +2\sigma_{xy}^{(i)}.\varepsilon_{xy}^{(i)}\Big)\Big]\, dy\, dx \qquad (4)$$

$$W = \sum_{i=1,2,\alpha} W_i \frac{1}{2}\int_0^l [D_1(\sigma_1)^2 + D_2(\sigma'')^2 + D_3(\sigma_1\sigma_1'') + D_4(\sigma_1')^2 + D_5(\sigma_1) + D_6(\sigma_1'') + +D_7]\, dx = \cdots = \frac{1}{2}\int_0^1 \Phi\big(x, \sigma_{1,}\sigma_1', \sigma_1''\big)\, dx \qquad (5)$$

The minimum of complementary strain energy functional can be found according to Euler-Lagrange equation of the variational calculus. This equation leads to the following ODE of 4th order with constant coefficients $D_i$ :

$$2D_2\,\sigma_1^{IV} + (2D_3 - 2D_4)\sigma_1'' + 2D_1\sigma_1 + D_5 = 0 \quad (6)$$

The discriminant of the respective characteristic equation of Eq. (6) can be positive or negative, so the roots can be real or complex numbers or mixed. Additional conditions to obtain four real or complex or mixed roots for bi-quadratic characteristic equation of (6) has to be fulfilled for its coefficients (details could be found in [34]). Here, the sign of discriminant depends on coefficients $D_i$ - Eq.(6a) or, on the thicknesses and material properties of the structure layers:

$$D_1 = \frac{h_1}{E^{(1)}} + \frac{h_2\rho^2}{E^{(2)}}$$

$$D_2 = \frac{h_1^5}{20E^{(1)}} + \frac{h_1^2 h_2}{120E^{(2)}}\left[\begin{array}{l} 6h_2^2 - 15h_2\left(y_t + h_\alpha\right) \\ +10\left(y_t + h_\alpha\right)^2 \end{array}\right] + \frac{h_1^2 h_\alpha}{12E^{(2)}}\left[3h_1^2 + 6h_1h_\alpha + 4h_\alpha^2\right] \quad (6a)$$

$$D_3 = -\frac{\nu^{(1)}h_1^3}{3E^{(1)}} - \frac{\rho\nu^{(2)}h_1h_2\left[2h_2 - 3\left(y_t + h_\alpha\right)\right]}{6E^{(2)}}$$

$$D_4 = \frac{2}{3}\frac{\left(1+\nu^{(1)}\right)h_1^3}{E^{(1)}} + \frac{2}{3}\frac{\left(1+\nu^{(2)}\right)}{E^{(2)}}h_1^2h_2 + \frac{2\left(1+\nu^{(\alpha)}\right)h_1^2h_\alpha}{E^{(2)}}$$

$$D_5 = (\alpha^{(1)} - \alpha^{(2)})\Delta T.h_1 - \frac{2h_2\rho\sigma_0}{E^{(2)}}$$

In Eq. (6a) $\alpha^{(i)}, i = 1, \alpha, 2$ are the coefficients of thermal expansion of the layers, ΔT is the temperature difference, and $y_t = h_1 + h_2 + h_a$. The temperature T is supposed to be uniformly distributed in the layers.

The general solutions for $\sigma_1$ for real $\lambda_i$ and complex roots $\pm(\alpha \pm i.\beta)$ are, respectively:

$$\sigma_1 = C_1 exp(\lambda_1 x) + C_2 exp(\lambda_2 x) + C_3 exp(\lambda_3 x) + C_4 exp(\lambda_4 x) - A \quad (7)$$

$$\sigma_1 = exp(-\alpha x)(\mathrm{M}_1\cos(\beta x) + \mathrm{M}_2\sin(\beta x)) + exp(\alpha x)(\mathrm{M}_3\cos(\beta x) + \mathrm{M}_4\sin(\beta x)) - A \quad (8)$$

Constant $A = D_5/2D_1$ in the solutions depends on the value of external static load $\sigma_0$ and ΔT; practically, it is a partial solution of the non-homogeneous Eq. (6). The coefficients $M_i, C_i$ are integration constants in the model solution, determined from the boundary conditions. After obtaining the solution for $\sigma_1$, all stresses in the layers (axial, normal (peel) and shear stresses) are determined as functions of $\sigma_1$ and its derivatives (see Eqs. (1) ÷ (3)).

Finally, the 2D strains in the structure layers can be obtained as:

$$\varepsilon_{xx}^{(i)} = \frac{1}{E^{(i)}}\sigma_{xx}^{(i)} - \frac{\nu^{(i)}}{\mathrm{E}^{(i)}}\sigma_{yy}^{(i)} + \varepsilon_{\mathrm{T}_{xx}}^{(i)},$$
$$\varepsilon_{yy}^{(i)} = -\frac{\nu^{(i)}}{\mathrm{E}^{(i)}}\sigma_{xx}^{(i)} + \frac{1}{\mathrm{E}^{(i)}}\sigma_{yy}^{(i)} + \varepsilon_{T_{yy}}^{(i)},$$
$$\varepsilon_{xy}^{(i)} = \frac{1 + \nu^{(i)}}{E^{(i)}}\sigma_{xy}^{(i)},$$
$$\varepsilon_{T_{xx}}^{(i)} = \alpha_x^{(i)}\Delta T, \quad \varepsilon_{\mathrm{T}_{yy}}^{(i)} = \alpha_y^{(i)}\Delta T \quad (9)$$

## RESULTS AND DISCUSSION

### *Numerical example*

The structure's material and geometric properties in the numerical example are according to the data in [16] and are given in Table 1. The structure length is $l$=20 μm, $\Delta T = T - T_0$ = 50 K, starting from room temperature $T_0$ (RT). The applied load is 15 MPa, if not stated otherwise.

**Table 1.** Structure material and geometrical properties.

| Geometry and physical properties | Layer 1, Graphene | Layer 2, PMMA | Layer Adhesive, SU-8 |
|---|---|---|---|
| Thickness of the layer $h_i$, m | 1.002e-09 | 1.5e-06 for (7)/ 30e-06 for (8) | 300e-09 |
| Young's modulus $E$, Pa | 1e+12 | 3.5e+09 | 2e+09 |
| Poisson's ratio ν, - | 0.13 | 0.25 | 0.22 |
| Coefficient of thermal expansion $\alpha_i$ (CTE), 1/K | -8e-06 | 74e-06 | 52e-06 |

For the model strains calculation and figures plot preparation, Mathcad Prime v.6.0 and Sigma Plot, v.13.0 were used, respectively.

From Figs. 2÷4, it can be concluded that applying a thermal loading (ΔT > 0) to a mechanical one, the resultant thermomechanical strains $\varepsilon_{xx}^{(i)}, \varepsilon_{xy}^{(i)}, \varepsilon_{yy}^{(i)}$, ($i$ =1,a,2) have the same behavior like the mechanical

ones, with increasing magnitude in the same range as that of mechanical ones (cases (a÷c) in Figs. 2-4).

For the axial $\varepsilon_{xx}^{(i)}$ and peel $\varepsilon_{yy}^{(i)}$ thermomechanical strains this rise in the amplitude is better visible than for the respective thermomechanical shear strains. The obtained results for the influence of temperature on the axial and peel strains are fully in agreement with recently published FEM results of Banarouei [31] for graphene/PMMA nanocomposites under temperature influence.

It should be noted that, to the best of the authors' knowledge, this [31] is the first appearance of data (experimental or model results), related to the distribution of stresses and strains in graphene as a function of temperature change.

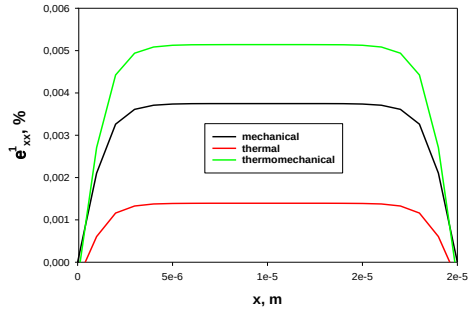


(a)

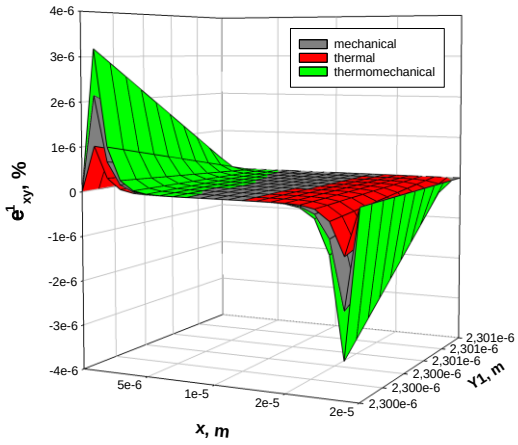


(a) (a)

(b)

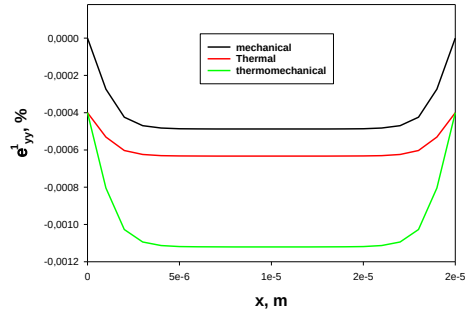


(c)

**Fig. 2.** Comparison of the axial strains (a), shear strains (b) and peel strains (c) in the graphene layer of the nanocomposite structure at different type of loading.

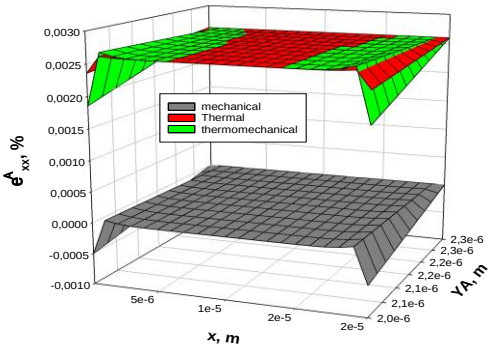


(a)

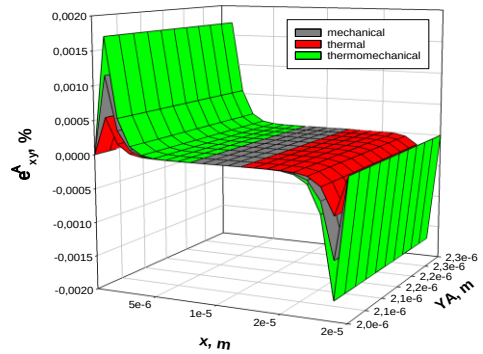


(b)

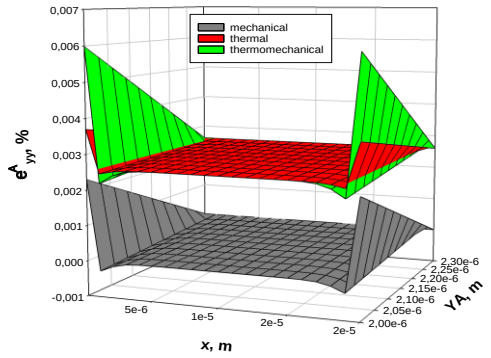


(c)

**Fig. 3.** Comparison of the axial strains (a), shear strains (b), and peel strains (c) in the adhesive layer of the nanocomposite structure at different type of loading.

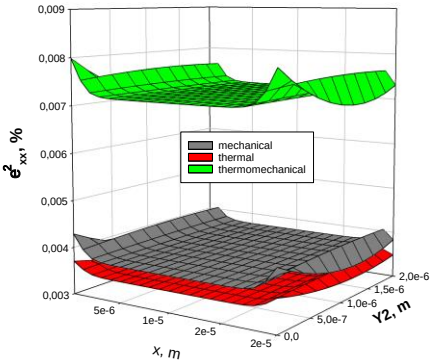


(a)

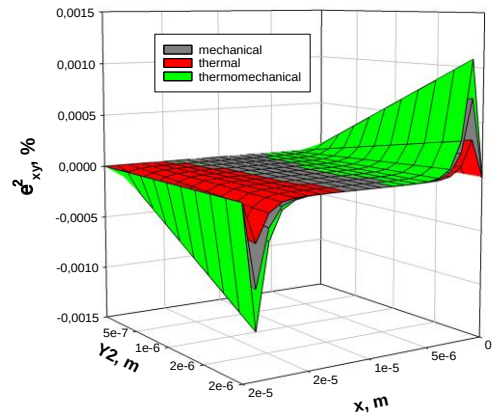


(b)

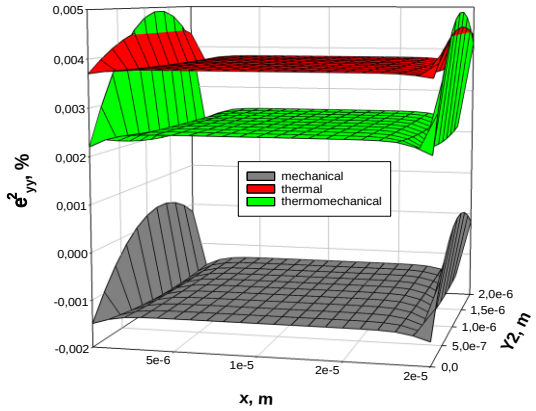


(c)

**Fig. 4.** Comparison of the axial strains (a), shear strains (b) and peel strains (c) in the PMMA layer of the nanocomposite.

On Figs. 5 and 6 the model axial strain in the graphene layer at two different mechanical external strains - 0.3% and 0.8%, was compared and validated with experimental data at mechanical loading from Androulidakis *et al*. [16].

The corresponding applied mechanical loads in our model for these two external strains 0.3 and 0.8 %, are 15 MPa and 1 GPa, respectively. As can be seen, our results fit well the experimental data, especially in the central part of the strain distribution along the flake length for both external strains. The mean relative errors (%) between our predictions and experimental data are 18 and 24 %, respectively, for Figs. 5 and 6; the largest deviations are due to the experimental data behavior near the flake edges, which are well visible on both figures. The proposed here model solution for strain in graphene suggests that at the ends of the flake the strain should be 0, while from experimental data distribution the opposite follows. In [33] this behavior near the graphene edges was investigated and explained as "…the distribution of axial stress (strain) along the flake deviates somewhat from the classical shear-lag prediction for a region of 1−2 μm from the edge". It was established [33], that this behavior is mainly attributed to the presence of residual stresses, unintentional doping, and/or edge effects.

Nevertheless, the maximum values of the strain's plateau were predicted with very good accuracy as is well visible in Figs. 5 and 6. This, as well as the agreement of our predictions with the results in [31], confirm our model validity and usage for future prognosis of stresses and strains distributions in similar nanocomposite structures subjected to thermomechanical loading.

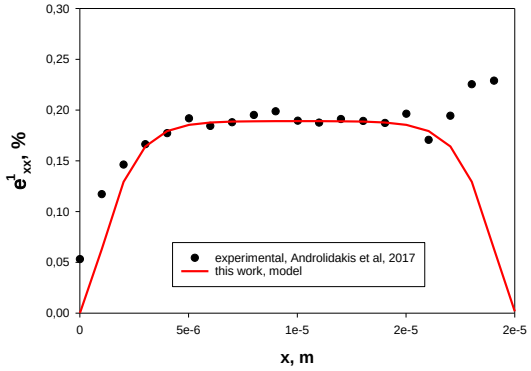


**Fig. 5**. Comparison of the model axial strains in the graphene layer of the nanocomposite structure at mechanical external strain 0.3% with experimental data of Androulidakis *et al*., 2017 [16].

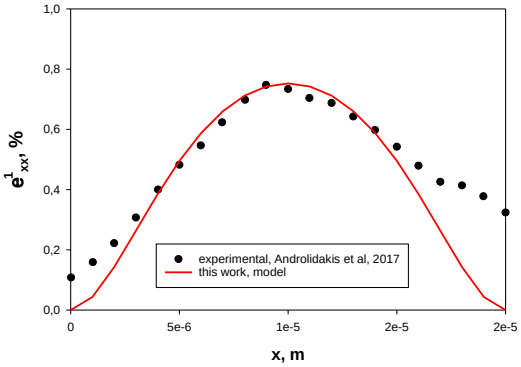


**Fig. 6.** Comparison of the model axial strains in the 1st layer of the nanocomposite structure at mechanical external strain 0.8 % with experimental data of Androulidakis *et al*., 2017 [16].

## CONCLUSIONS

In this study, the applicability of a two-dimensional stress-function method for describing strains in nanocomposite layered structures in the elastic region of applied loads is shown. Applying a thermal loading (heating, $\Delta T > 0$) or mixed (thermomechanical) loading, all resultant strains in the structure layers show the same behavior like mechanical ones, with slight increase in amplitude. This is better visible for axial and peel strains, as in [31]. Comparison of the model axial strains in the 1st layer of the nanocomposite structure at mechanical

external strain of 0.3% and 0.8% with the experimental data of Androulidakis *et al*. [16] shows that our results fit well most of the experimental data distribution. The experimental deviations near the flake ends may be due to the presence of residual stresses, unintentional doping, and/or edge effects [33].

***Acknowledgements:*** *The authors gratefully acknowledge the Bulgarian National Science Fund for its financial support via the contract for project КП-06-Н57/3/15.11.2021.*

REFERENCES

1. H. Kim, A. A. Abdala, C. W. Macosko, *Macromolecules*, **43**, 6515 (2010).
2. X. Sun, C. Huang, L. Wang, L. Liang, Y. Cheng, W. Fei, Y. Li, *Adv. Mater*., Article 2001105 (2020).
3. K. Rege, N. R. Raravikar, D.-Y. Kim, L. S. Schadler, P. M. Ajayan, J. S. Dordick, *Nano Lett*., **3** (6), 829 (2003).
4. R. Atif, F. Inam, *Graphene*, **5** (2), 96 (2016).
5. F. Lin, Y. Xiang, H.-S. Shen, *Composites Part B*, **111**, Article 261e269 (2017).
6. B. Mortazavi, T. Rabczuk, *Carbon*, **85**, 1 (2015).
7. P. Popova-Krumova, Chr. Boyadjiev, in: Modeling and Simulation in Chemical Engineering, Project Reports on Process Simulation, Chr. Boyadjiev (ed.), Springer Nature, Switzerland, 2022, p. 199, ISBN:978-3-030-87659-3. https://doi.org/10.1007/978-3-030-87660-9
8. Chr. Boyadjiev, P. Popova-Krumova, in: Progress in Chemical Science Research, O. J. R. Baena (ed.), vol. 2, BP International, Hooghly, West Bengal, India, 2022, p. 1. https://doi.org/10.9734/bpi/pcsr/v2/1920A
9. G. Allegra, G. Raos, M. Vacatello, *Progress in Polymer Science*, **33** (7), 683 (2008).
10. G. Dai, L. Mishnaevsky, *Computational Materials Science*, **95**, 684 (2014).
11. Z. Dai, G. Wang, L. Liu, Y. Hou, Y. Wei, Z. Zhang, *Composites Science and Technology*, **136**, 1 (2016).
12. Y. Y. Jia, Z. R. Chen, W. Y. Yan, *Composites Science and Technology*, **91**, 38 (2014).
13. F. Toth, F. G. Rammerstorfer, M. J. Cordill, F. D. Fischer, *Acta Mater*., **61**(7), 2425 (2013).
14. A. P. Sgouros, C. Androulidakis, G. Tsoukleri, G. Kalosakas, N. Delikoukos, S. Signetti, N. M. Pugno, J. Parthenios, C. Galiotis, K. Papagelis, *ACS Appl. Mater. Interfaces*, **13**, 4473 (2021).
15. Ch. Androulidakis, E. N. Koukaras, M. G. P. Carbone, M. Hadjinicolaou, C. Galiotis, *Nanoscale*, **9**, Article 18180 (2017a).
16. Ch. Androulidakis, E.N. Koukaras, J. Rahova, K. Sampathkumar, J. Parthenios, K. Papagelis, O. Frank, C. Galiotis, *Nanoscale*, **9**, Article 26593 (2017b).
17. H. Kumar, L. Dong, V. B. Shenoy, *Scientific Reports*, **6**, Article 21516 (2016).
18. L. Gong, I. A. Kinloch, R. J. Young, I. Riaz, R. Jalil, K. S. Novoselov, *Adv. Mater*., **22**(24), 2694 (2010).
19. R. J. Young, I. A. Kinloch, L. Gong, K. S. Novoselov, *Composites Science and Technology*, **72** (12), 1459 (2012).
20. T. Jiang, R. Huang, Y. Zhu, *Adv. Funct. Mater*., **24**(3), 396 (2014).
21. S. Wang, Y. Chen, Y. Ma, Z. Wang, J. Zhang, *Journal of Applied Physics*, **122**, Article 074301 (2017).
22. T. Petrova, E. Kirilova, W. Becker, J. Ivanova, *IOP Conference Series: Materials Science and Engineering*, **461**(1), Article 012067 (2018).
23. E. Kirilova, T. Petrova, W. Becker, J. Ivanova, *IOP Conference Series: Materials Science and Engineering*, **461**(1), Article 012029 (2018).
24. H. Zhao, N. R. Aluru, *J. Appl. Phys.*, **108**, Article 064321 (2010).
25. M. A. N. Dewapriya, A. S. Phani, R. K. N. D. Rajapakse, *Modelling Simul. Mater. Sci. Eng*., **21**, Article 065017 (2013).
26. M. Takamura, H. Hibino, H. Yamamoto, *Journal of Physics D: Applied Physics*, **49**, Article 285303 (2016).
27. H.-S. Shen, Y. Xiang, F. Lin, D. Hui, *Composites Part B*, **119**, Article 67e78 (2017).
28. Y. Pan, B. Yang, N. Jia, Y. Yu, X. Xu, Y. Wang, B. Wu, J. Qian, R. Xia, C. Wang, A. Sun, Y. Shi, *Polymer Testing*, **101**, Article 107237 (2021).
29. Y. Yu, J. Wang, *Ultrasonics Sonochemistry*, **73**, Article 105487 (2021).
30. K. S. Kwok, Master thesis, Johns Hopkins University, Baltimore, Maryland, USA (2017).
31. S. A. Banarouei, Master thesis, York University, Toronto, Ontario, Canada (2021).
32. T. S. Petrova, E. G. Kirilova, W. Becker, J. A. Ivanova, *ZAMM*, Article e202200266 (2022). https://doi.org/10.1002/zamm.202200266
33. G. Anagnostopoulos, C. Androulidakis, E. N. Koukaras, G. Tsoukleri, I. Polyzos, J. Parthenios, K. Papagelis, C. Galiotis, *ACS Appl. Mater. Interfaces*, **7**, 4216 (2015).
34. A. D. Polyanin, V. F. Zaitsev, Handbook of exact solutions for ordinary differential equations, 2nd edn., 2002, Chapman & Hall/CRC, ISBN 9781584882978, Chapter 4. https://doi.org/10.1201/ 9781420035339